Oscillatory pattern selection by spatial heat release modulation in multistable Marangoni convection

Alexander A. Nepomnyashchy and Ilya B. Simanovskii
Department of Mathematics, Technion—Israel Institute of Technology, 32000 Haifa, Israel

(Received 23 February 2019; published 3 September 2019)

The action of spatial modulation of the Marangoni number, corresponding to the heat source or sink at the interface on wave patterns, has been studied. The analysis is carried out in the lubrication approximation. Numerical simulations are performed by means of a finite-difference method. It is found that in the case of multistability, the spatial heat release modulation can be used for the creation of a pattern with a definite spatial structure. It is shown that the violation of the reflection symmetry of the pattern by its spatial modulation can lead to a quasiperiodic temporal evolution.

DOI: 10.1103/PhysRevFluids.4.094001

I. INTRODUCTION

Nonlinear patterns created by instabilities have been a subject of extensive study for a few decades [1]. The nonlinear dynamics of systems subjected to oscillatory instabilities is especially rich [2]. For nonlinear patterns, a multistability is characteristic; specifically, in spatially extended systems different pattern planforms are possible. An important problem is controlling the development of instability, i.e., the suppression of undesired kinds of patterns or generation of a desired kind of pattern [3,4]. A possible way of controlling the pattern selection is a spatial modulation of the control parameter.

The very idea of multiple pattern generation by introducing a spatially inhomogeneous perturbation was first implemented in experiments of Chen and Whitehead [5], where stationary roll-like convection patterns were created by nonuniform heating. Since that time, the action of a spatially periodic forcing on the onset of stationary patterns has been explored extensively [6–14]. However, the action of stationary spatial modulation on the oscillatory pattern is less straightforward. It has been studied mostly near the oscillatory instability threshold in the framework of the complex Ginzburg-Landau equation [15–20]. Direct numerical simulations of nonlinear Marangoni waves under the action of a spatial temperature modulation have been carried out recently [21].

In the present paper, we investigate the possibility of the generation of different oscillatory patterns by means of spatially inhomogeneous perturbations. We consider the deformational oscillatory Marangoni convection in a two-layer film in the presence of a transverse temperature gradient and a heat release or consumption at the liquid-liquid interface, previously studied in [22]. Unlike most of the former investigations of the two-layer Marangoni convection, where it is typically assumed that heating or cooling is carried out solely through the substrate or the free surface while the normal components of the heat flux are equal on both sides of the interface between the fluids, we include a spatially inhomogeneous heat source or sink on the interface. The interfacial heating can be generated, e.g., by an infrared light source. The infrared absorption bands of different liquids can be essentially different [23], and therefore the light frequency can be chosen in a way that one of the liquids is transparent, while the characteristic length of the light absorption in another liquid is short. Note that fluid flows generated by infrared heating were studied experimentally in [24].

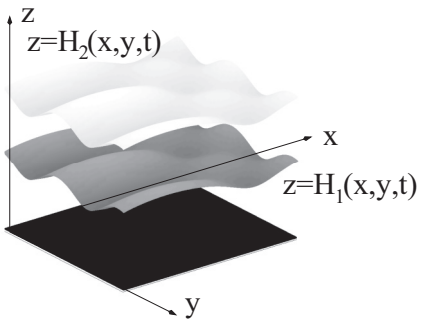

FIG. 1. Geometric configuration of the region and coordinate axes.

The formulation of the problem is given in Sec. II. The system of long-wave-amplitude equations governing the evolution of surface deformations is presented in Sec. III. Section IV contains the description of the numerical method. In Sec. V we discuss the possibility of the creation of a prescribed pattern by interfacial heat release-consumption modulation. The results of nonlinear simulations of patterns in the presence of spatially inhomogeneous perturbations are described in Sec. VI. We summarize in Sec. VII.

II. FORMULATION OF THE PROBLEM

Consider a system of two superposed layers of immiscible liquids with different physical properties (see Fig. 1). The bottom layer rests on a solid substrate and the top layer is in contact with the adjacent gas phase. All the variables referring to the bottom layer are marked by subscript 1 and all the variables referring to the top layer are marked by subscript 2. The equilibrium thicknesses of the layers are H_m^0, $m = 1, 2$. The deformable interfaces are described by the equations $z = H_1(x, y, t)$ (liquid-liquid interface) and $z = H_2(x, y, t)$ (liquid-gas interface).

The mth fluid has density ρ_m, dynamic viscosity η_m, thermal diffusivity χ_m, and heat conductivity κ_m. The temperature of the solid substrate is T_s and the temperature of the gas near the interface is T_g. At the interface, there is a heat source or sink which creates a jump $Q_*(x, y)$ of the normal heat flux. The surface tension coefficients on the lower and upper interfaces, σ_1 and σ_2, are linear functions of the temperature T: $\sigma_1 = \sigma_1^0 - \alpha_1 T$ and $\sigma_2 = \sigma_2^0 - \alpha_2 T$. The effect of gravity and the intermolecular forces are neglected.

The Marangoni convection is governed by the following system of nonlinear equations [25]:

$$\rho_m\left[\frac{\partial \mathbf{v}_m}{\partial t} + (\mathbf{v}_m \cdot \nabla)\mathbf{v}_m\right] = -\nabla P_m + \eta_m \Delta \mathbf{v}_m, \tag{1}$$

$$\frac{\partial T_m}{\partial t} + \mathbf{v}_m \cdot \nabla T_m = \chi_m \Delta T_m, \tag{2}$$

$$\nabla \cdot \mathbf{v}_m = 0, \quad m = 1, 2. \tag{3}$$

Here P_m is the difference between the actual pressure and the gas uniform pressure; $\mathbf{v}_m$ is the velocity in the mth liquid.

The dynamic boundary conditions on the deformable interface $z = H_1$ are

$$P_2 - P_1 + 2\sigma_1 K_1 = \left[-\eta_1\left(\frac{\partial v_{1i}}{\partial x_k} + \frac{\partial v_{1k}}{\partial x_i}\right) + \eta_2\left(\frac{\partial v_{2i}}{\partial x_k} + \frac{\partial v_{2k}}{\partial x_i}\right)\right] n_{1i} n_{1k}, \quad i, k = 1, 2, 3, \tag{4}$$

where K_1 is the mean curvature of the interface (condition for the normal stress balance), and

$$\left[-\eta_1\left(\frac{\partial v_{1i}}{\partial x_k}+\frac{\partial v_{1k}}{\partial x_i}\right)+\eta_2\left(\frac{\partial v_{2i}}{\partial x_k}+\frac{\partial v_{2k}}{\partial x_i}\right)\right]\tau_{1i}^{(l)}n_{1k}-\alpha_1\tau_{1i}^{(l)}\frac{\partial T_1}{\partial x_i}=0,\quad l=1,2;\quad i,k=1,2,3 \tag{5}$$

(conditions for the tangential stress balance). Here $\mathbf{n}_1$ is the normal vector and $\boldsymbol{\tau}_1^{(l)}$, $l=1,2$, are orthogonal tangential vectors. In the quantities with two subscripts, the first subscript corresponds to the liquid ($m=1,2$) and the second subscript determines the number of the Cartesian coordinate ($i,k=1,2,3$; $x_1=x$, $x_2=y$, and $x_3=z$). The usual summation convention is applied. Also, the kinematic boundary condition is imposed:

$$\frac{\partial H_1}{\partial t}+v_{1x}\frac{\partial H_1}{\partial x}+v_{1y}\frac{\partial H_1}{\partial y}=v_{1z}. \tag{6}$$

Across the interface, the fields of velocity and temperature are continuous:

$$\mathbf{v}_1=\mathbf{v}_2,\quad T_1=T_2. \tag{7}$$

Due to the interfacial heat release or consumption, there is a jump of the normal heat flux density,

$$\left(\kappa_1\frac{\partial T_1}{\partial x_i}-\kappa_2\frac{\partial T_2}{\partial x_i}\right)n_{1i}=Q_*(x,y). \tag{8}$$

The boundary conditions on the deformable surface $z=H_2$ are

$$-P_2+2\sigma_2K_2=-\eta_2\left(\frac{\partial v_{2i}}{\partial x_k}+\frac{\partial v_{2k}}{\partial x_i}\right)n_{2i}n_{2k}, \tag{9}$$

$$-\eta_2\left(\frac{\partial v_{2i}}{\partial x_k}+\frac{\partial v_{2k}}{\partial x_i}\right)\tau_{2i}^{(l)}n_{2k}-\alpha_2\tau_{2i}^{(l)}\frac{\partial T_3}{\partial x_i}=0,\ l=1,2;\quad i,k=1,2,3 \tag{10}$$

$$\frac{\partial H_2}{\partial t}+v_{2x}\frac{\partial H_2}{\partial x}+v_{2y}\frac{\partial H_2}{\partial y}=v_{2z}, \tag{11}$$

$\mathbf{n}_2$ is the normal vector, $\boldsymbol{\tau}_2^{(l)}$ ($l=1,2$) are the tangential vectors of the upper surface, and K_2 is the mean curvature. For a heat flux on the liquid-gas interface we use an empirical condition

$$\kappa_2\frac{\partial T_2}{\partial x_i}n_{2i}=-q(T_2-T_g), \tag{12}$$

where q is the heat exchange coefficient which is assumed to be constant. The boundary conditions on the rigid boundary $z=0$ are

$$\mathbf{v}_1=0,\quad T_1=T_s. \tag{13}$$

III. LONG-WAVE-AMPLITUDE EQUATIONS

The system of equations and boundary conditions (1)–(13) is rather complicated. However, the problem can be drastically simplified by using long-wavelength expansions in the case where the characteristic spatial scale of the interfacial heat release-consumption modulation is much larger than the thickness of the layer, i.e., the temperature modulation depends on the scaled coordinates $\tilde{X}=\epsilon x$ and $\tilde{Y}=\epsilon y$, $\epsilon\ll 1$, rather than on x and y. Later on, we assume that the solution of equations and boundary conditions (1)–(13) *itself* depends only on the slow variables $\tilde{\mathbf{X}}=(\tilde{X},\tilde{Y})$. Also, it is assumed that the solution depends on the scaled time variable $\tilde{\tau}=\epsilon^2 t$. These assumptions are justified in the case of a strong surface tension. The strong surface tension suppresses shortwave deformations of the surfaces; therefore the instability takes place only in the region of long waves. Later on, we assume that $\sigma_m=\sigma_m^0\epsilon^{-2}$ and $\sigma_m^0=O(1)$, $m=1,2$. Also, we assume that the dependence of interfacial tensions on the temperature is relatively weak and can

be neglected in the boundary conditions for normal stresses (but not in those for tangential stresses where it is the source of a thermocapillary motion). The details of the long-wave approach applied to thermocapillary flows can be found in review papers [26,27].

The application of the long-wave approach leads to a closed system of equations that govern the evolution of a heated two-layer film:

$$H_{1\tau} + \tilde{\nabla} \cdot \mathbf{Q}_1 = 0, \quad H_{2\tau} + \tilde{\nabla} \cdot \mathbf{Q}_2 = 0. \tag{14}$$

A detailed derivation of (14) in the case of the spatially homogeneous interfacial heat release or consumption is given in [22]. The derivation in the case of spatial modulation is quite similar, and hence we omit it here and present only the final results.

While the natural vertical length scale is the mean thickness of the lower layer H_1^0, the horizontal length scale L^* is arbitrary (see [28]). We choose

$$\tau^* = \frac{\eta_1 (L^*)^4}{\sigma_1^0 \left(H_1^0\right)^3} \tag{15}$$

as a time scale,

$$p^* = \frac{\sigma_1^0 H_1^0}{(L^*)^2} \tag{16}$$

as a pressure scale, and $|T_s - T_g|$ as the temperature scale. We define nondimensional variables

$$\mathbf{X} = \tilde{\mathbf{X}}/L^*, \quad \tau = \tilde{\tau}/\tau^*;$$
$$h_j = H_j/H_1^0, \quad p_j = P_j/p^*, \quad j = 1, 2$$

and introduce the following set of nondimensional parameters: $\eta = \eta_1/\eta_2$, $\kappa = \kappa_1/\kappa_2$, $\sigma = \sigma_2^0/\sigma_1^0$, $\alpha = \alpha_2/\alpha_1$, and $h = H_2^0/H_1^0$. Also, we define the Biot number

$$\mathrm{Bi} = \frac{qH_1^0}{\kappa_2}. \tag{17}$$

Because there are two independent sources of temperature inhomogeneity, the temperature difference across the film and interfacial heating or cooling, the thermocapillary convection in the system is characterized by two different Marangoni numbers

$$M = \frac{\alpha_1 (T_s - T_g)}{\sigma_1^0} \left(\frac{L_*}{H_1^0}\right)^2 \tag{18}$$

and

$$M_Q = \frac{\alpha_1 Q_* (L_*)^2}{\sigma_1^0 H_1^0 \kappa_2}. \tag{19}$$

Note that the Marangoni number M_Q, corresponding to the heat source or sink at the interface, is a function of the coordinate $\mathbf{X}$,

$$M_Q = M_Q(\mathbf{X}).$$

Equations (14) written in the nondimensional form look like

$$h_{1\tau} + \nabla \cdot \mathbf{q}_1 = 0, \quad h_{2\tau} + \nabla \cdot \mathbf{q}_2 = 0, \tag{20}$$

where

$$\mathbf{q}_j = \mathbf{q}_j^T + \mathbf{q}_j^\sigma, \quad j = 1, 2$$
$$\mathbf{q}_1^T = \frac{M}{2} h_1^2 \nabla [d(\mathrm{Bi} h_1 - \alpha\kappa)] - \frac{1}{2} h_1^2 \nabla \{M_Q d h_1 [1 + \alpha + \mathrm{Bi}(h_2 - h_1)]\}, \tag{21}$$

$$\mathbf{q}_2^T = \frac{M}{2}\left(-h_2^2\nabla(d\eta\alpha\kappa) + (2h_2 - h_1)h_1\nabla\{d[\mathrm{Bi}h_1 - \alpha\kappa(1-\eta)]\}\right)$$
$$- \frac{1}{2}[(1+\alpha)h_1(2h_2 - h_1) + \eta\alpha(h_2 - h_1)^2]\nabla(M_Q d h_1)$$
$$- \frac{\mathrm{Bi}}{2}h_1(2h_2 - h_1)\nabla[M_Q d h_1(h_2 - h_1)], \tag{22}$$

$$d(\mathbf{X},\tau) = [\kappa + \mathrm{Bi}(1-\kappa)h_1(\mathbf{X},\tau) + \mathrm{Bi}\kappa h_2(\mathbf{X},\tau)]^{-1}. \tag{23}$$

The nondimensional expressions for $\mathbf{q}_1^\sigma$ and $\mathbf{q}_2^\sigma$ are

$$\mathbf{q}_1^\sigma = f_{11}\nabla p_1 + f_{12}\nabla p_2, \quad \mathbf{q}_2^\sigma = f_{21}\nabla p_1 + f_{22}\nabla p_2, \tag{24}$$

where the nondimensional mobilities are

$$f_{11} = -\frac{1}{3}h_1^3, \quad f_{12} = -\frac{1}{2}h_1^2(h_2 - h_1), \quad f_{21} = \frac{1}{6}h_1^3 - \frac{1}{2}h_1^2 h_2,$$
$$f_{22} = -(h_2 - h_1)\left[\frac{1}{2}h_1(2h_2 - h_1) + \frac{\eta}{3}(h_2 - h_1)^2\right]$$

and the capillary pressures are

$$p_1 = -\nabla^2 h_1 - \sigma\nabla^2 h_2, \tag{25}$$

$$p_2 = -\sigma\nabla^2 h_2. \tag{26}$$

IV. NUMERICAL METHOD

We have performed nonlinear simulations of Eqs. (20) with a spatially periodic modulation of the Marangoni number M_Q corresponding to the heat source or sink at the interface,

$$M_Q(X + L, Y) = M_Q(X, Y + L) = M_Q(X, Y). \tag{27}$$

Let us emphasize that L is a nondimensional parameter; the dimensional modulation period is $\tilde{L} = LL^*$. Equations (20) have been discretized by central differences for spatial derivatives and solved using an explicit scheme. Initial conditions for h_j, $j = 1, 2$, have been chosen in such a way that the mean value of $h_1(X, Y, 0)$ was equal to 1 and the mean value of $h_2(X, Y, 0)$ was equal to h, where $h > 1$. Small random deviations of $h_j(X, Y, 0)$ from their mean values were imposed using a code creating pseudorandom numbers.

Unlike the case of short-wave instability, where the characteristic horizontal scale is determined by the linear stability theory as $\lambda_c = 2\pi/k_c$ (k_c is the critical wave number), in the case of a long-wave instability ($k_c = 0$) the problem has no characteristic horizontal scale except the size of the region. At large L, the characteristic scale of the pattern created by instability is of the order of L.

The computations have been performed in the region $L \times L = 240 \times 240$ with periodic boundary conditions. For moderate values of M and M_Q, the fields h_1 and h_2 are rather smooth, and thus the grid 80×80 gives a good resolution of large-scale wave patterns.

The primary analysis of the obtained nonlinear regimes has been performed using snapshots of the fields of $h_j(X, Y, \tau)$, $j = 1, 2$. This analysis has been supplemented by the investigation of the Fourier components

$$c_{mn}(\tau) = \frac{2}{L^2}\int_0^L\int_0^L h_1(X, Y, \tau)\cos\left[\frac{2\pi}{L}(mX + nY)\right]dX\,dY, \tag{28}$$

$$s_{mn}(\tau) = \frac{2}{L^2}\int_0^L\int_0^L h_1(X, Y, \tau)\sin\left[\frac{2\pi}{L}(mX + nY)\right]dX\,dY, \tag{29}$$

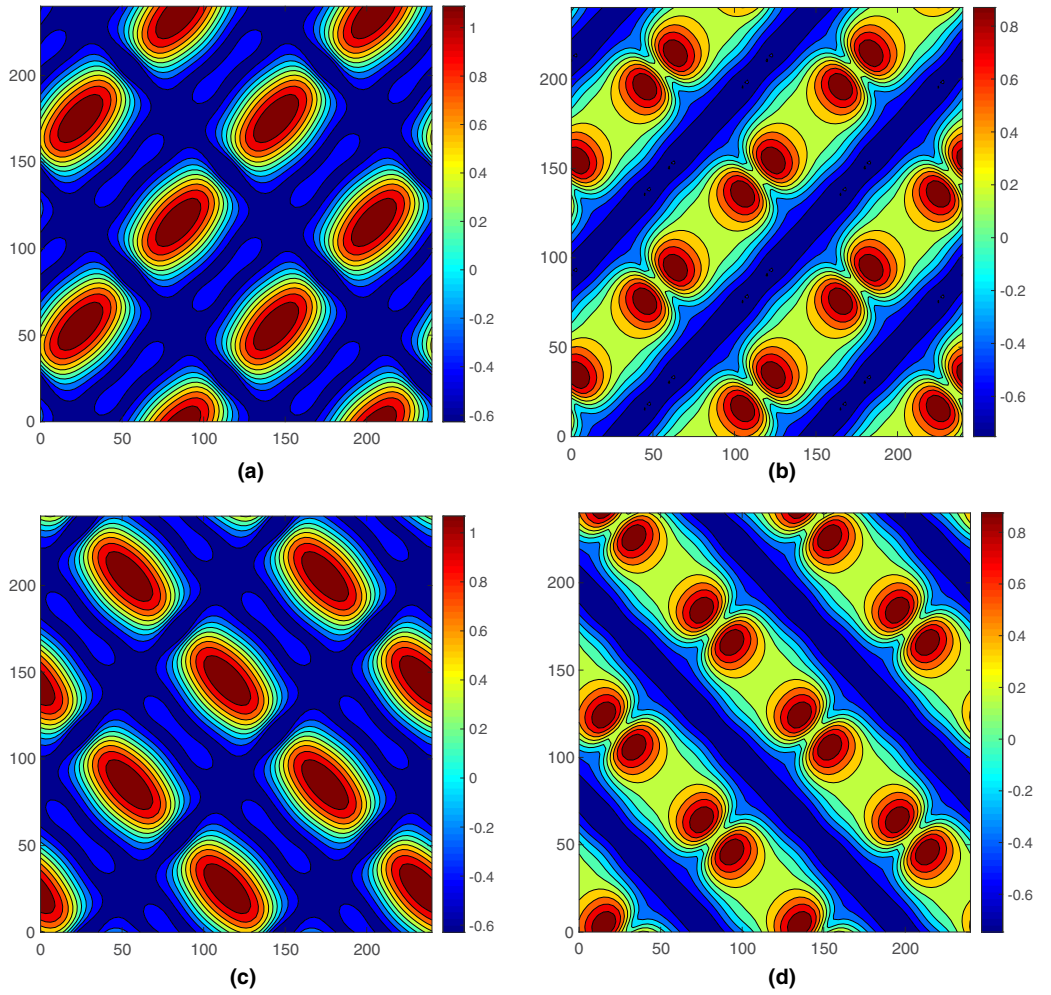

FIG. 2. Snapshots of contour lines of $h_1(X, Y, \tau) - 1$ for alternating rolls with basic wave vectors $(2k_0, 2k_0)$ and $(2k_0, -2k_0)$ (AR1) for $M = -2$, $M_Q = -0.5$, and (a) $\tau = 1\,200\,000$, (b) $\tau = 1\,200\,250$, (c) $\tau = 1\,200\,750$, and (d) $\tau = 1\,201\,000$.

where m and n are integer numbers. We have used also variables

$$r_{mn}(\tau) = \sqrt{c_{mn}^2(\tau) + s_{mn}^2(\tau)}, \tag{30}$$

characterizing the amplitudes of corresponding complex Fourier harmonics, and quantities

$$h_{\max,j}(\tau) = \max_{X,Y} h_j(X, Y, \tau), \quad j = 1, 2, \tag{31}$$

which describe the deformations of the surfaces.

V. PATTERN SELECTION BY INTERFACIAL HEAT RELEASE-CONSUMPTION MODULATION

Let us discuss the stability of the mechanical equilibrium and the nonlinear flow regimes in the case of homogeneous heating previously studied in [22,28]. It has been shown that in addition to a

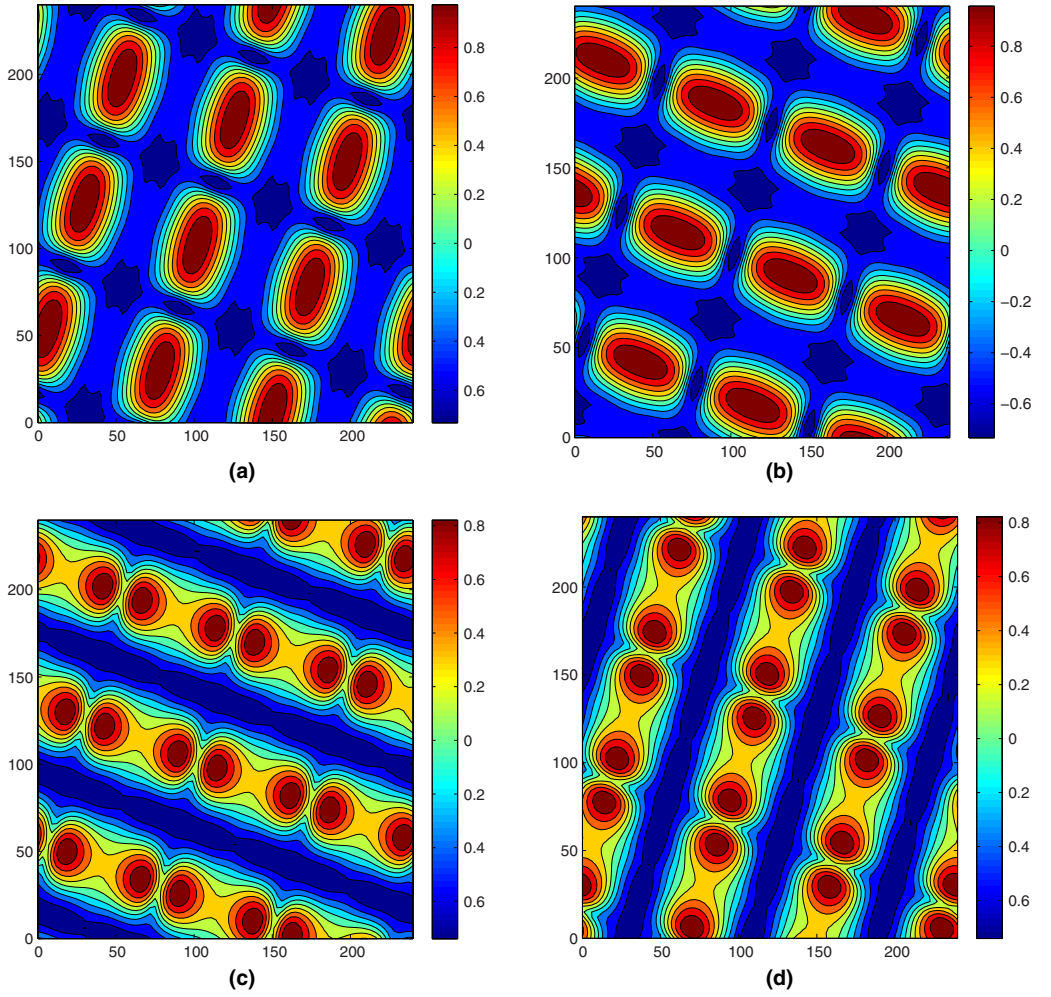

FIG. 3. Snapshots of contour lines of $h_1(X, Y, \tau) - 1$ for alternating rolls with basic wave vectors $(k_0, 3k_0)$ and $(3k_0, -k_0)$ (AR2) for $M = -2$, $M_Q = -0.5$, and (a) $\tau = 399\,003$, (b) $\tau = 399\,100$, (c) $\tau = 399\,300$, and (d) $\tau = 399\,400$.

monotonic instability leading to the rupture of the film, the two-layer film is subject to an oscillatory instability that generates self-sustained Marangoni waves. In the absence of the interfacial heat release or consumption, the oscillatory instability [with the growth rate $\lambda(k)$, $\mathrm{Re}\lambda(k) > 0$, and $\mathrm{Im}\lambda(k) \neq 0$] is developed by heating from below ($M > 0$) if $\mathrm{Bi} < \mathrm{Bi}_c$ and by heating from above ($M < 0$) if $\mathrm{Bi} > \mathrm{Bi}_c$, where

$$\mathrm{Bi}_c = \frac{1 + \alpha(1 + \eta\kappa a^2 + 2\kappa a)}{a};$$

here $a = h - 1$ (see [28]). As shown in [22], the oscillatory instability is retained in the presence of the interfacial heat release or consumption within a definite interval of the parameter

$$Q = \frac{M_Q}{M\,\mathrm{Bi}\kappa}.$$

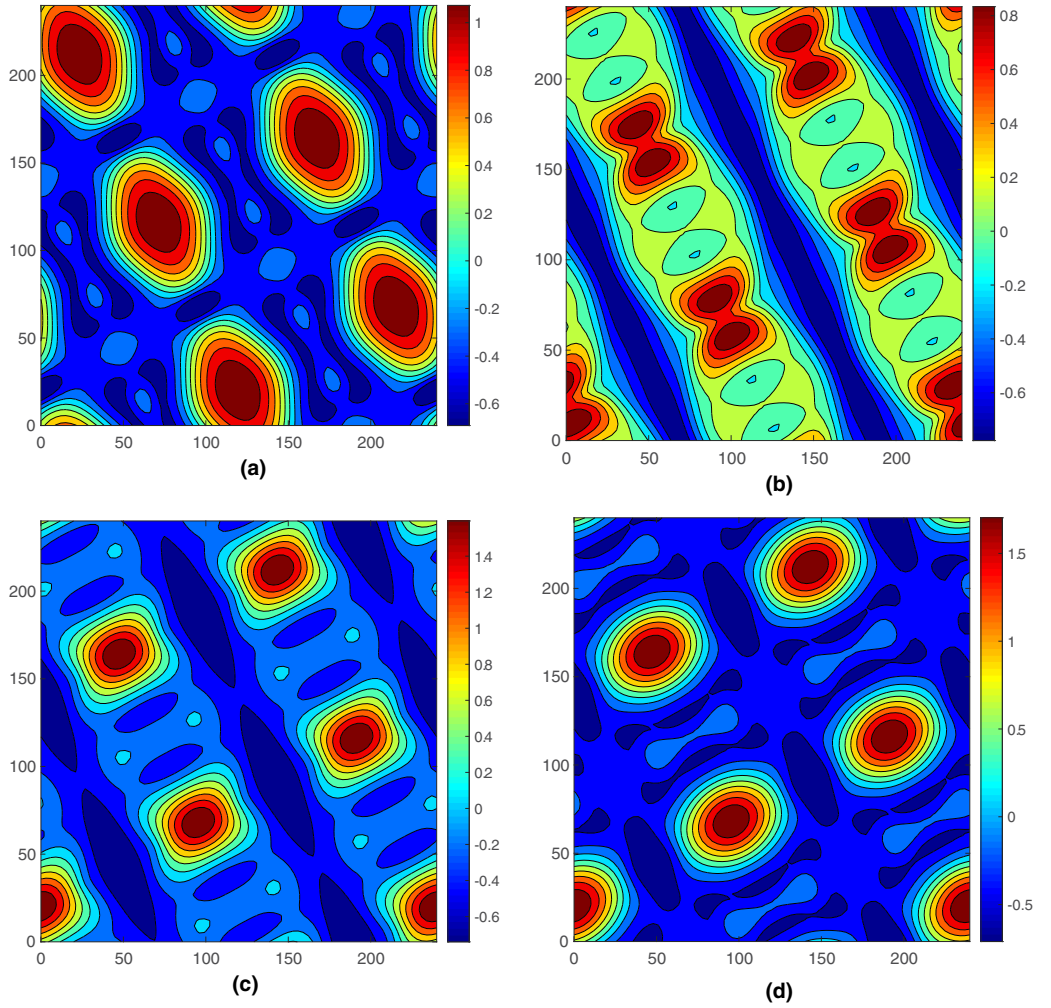

FIG. 4. Snapshots of contour lines of $h_1(X, Y, \tau) - 1$ for alternating rolls with basic wave vectors $(-k_0, 2k_0)$ and $(2k_0, k_0)$ (AR3) for $M = -2$, $M_Q = -0.5$, and (a) $\tau = 1\,200\,000$, (b) $\tau = 1\,200\,500$, (c) $\tau = 1\,200\,750$, and (d) $\tau = 1\,201\,000$.

Experimental observation of the oscillatory instability described above is lacking; the system of fluorinert and silicone oil is a good candidate for performing future experiments. It is one of the most typical pairs of liquids used in two-liquid experiments [29–32] for the following reasons: (i) Both liquids are almost immiscible and (ii) for different kinds of silicone oils, the viscosity changes over a wide range. In the present paper, we perform computations for a particular system of liquids, that of fluorinert FC70 (liquid 1) and silicone oil 10 (liquid 2), previously used in microgravity experiments (see, e.g., [31]). It is characterized by the following parameter values: $\eta = 3.04$, $\kappa = 0.522$, $\alpha = 2$, $\rho = 0.482$, $\sigma = 2.6$, $a = 1.5$, and $\mathrm{Bi} = 10$. For that system, the interval of oscillatory instability by heating from above is $-0.004\,97 < Q < 0.0710$ (see [22]). Below we set $M = -2$ and $M_Q = -0.5$ ($Q = 0.048$).

For the values of the parameters listed above, the real part $\mathrm{Re}\lambda(k)$ of the complex growth rate $\lambda(k)$ corresponding to oscillations with the wave number k is determined by the formula

$$\mathrm{Re}\lambda(k) = 0.142k^2 - 9.92k^4.$$

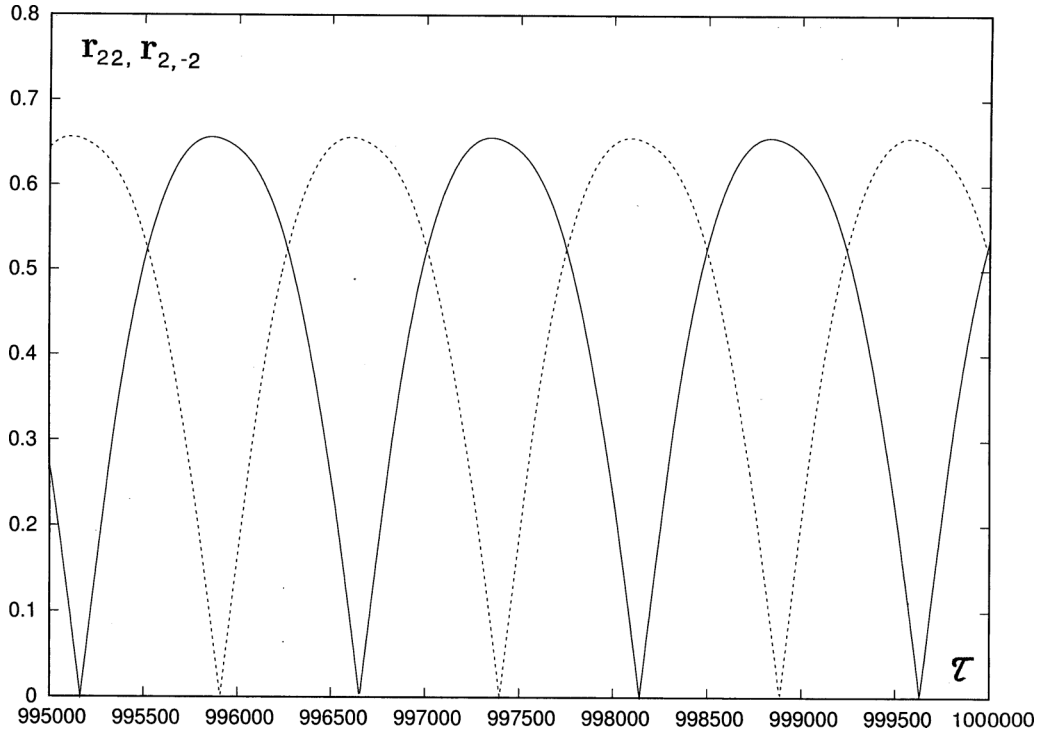

FIG. 5. Temporal evolution of amplitudes $r_{22}(\tau)$ (solid line) and $r_{2,-2}(\tau)$ (dashed line) for $M = -2$ and $M_Q = -0.5$ (pattern AR1).

Later on, we call it just the growth rate. Thus, any disturbances with wave numbers in the interval $0 < k^2 < k_*^2 \approx 0.143$ grow in time; the maximum growth rate corresponds to $k^2 = k_m^2 = k_*^2/2 \approx 0.718 \times 10^{-2}$.

In a finite region, the set of admissible wave vectors is discrete. The periodic boundary conditions on the boundaries of a finite computational region $0 \leqslant X \leqslant L$ and $0 \leqslant Y \leqslant L$ determine the set of admissible disturbance wave vectors

$$k_x = mk_0, \quad k_y = nk_0, \quad k_0 = 2\pi/L,$$

where m and n are integer numbers. For $L = 240$, we obtain $k_0^2 \approx 0.685 \times 10^{-3}$, hence $(k_m/k_0)^2 \approx 10.5$. Therefore, among all the admissible disturbances, the disturbances with $(m, n) = (\pm 1, \pm 3)$ and $(m, n) = (\pm 3, \pm 1)$ have the maximum growth rate $\lambda(10k_0^2) \approx 0.51 \times 10^{-3}$. For comparison, let us present also the growth rates for some other disturbances: For $(m, n) = (\pm 1, \pm 2)$ and $(m, n) = (\pm 2, \pm 1)$, $\lambda(5k_0^2) \approx 0.371 \times 10^{-3}$; for $(m, n) = (\pm 2, \pm 2)$, $\lambda(8k_0^2) \approx 0.483 \times 10^{-3}$; and for $(m, n) = (\pm 2, \pm 3)$ and $(m, n) = (\pm 3, \pm 2)$, $\lambda(13k_0^2) \approx 0.481 \times 10^{-3}$.

At fixed values of L, M, and M_Q, inside the interval $0 < k^2 < k_*^2$ determined by the linear stability theory, there exists a subinterval of stable nonlinear wave patterns satisfying the periodicity conditions. For instance, in the case when $L = 240$, $M = -2$, and $M_Q = -0.5$, alternating rolls with three different values of the wave number have been observed in numerical simulations: (i) alternating rolls with basic wave vectors $(2k_0, 2k_0)$ and $(2k_0, -2k_0)$ (AR1), $k^2 = 8k_0^2$ (see Fig. 2); (ii) alternating rolls with basic wave vectors $(k_0, 3k_0)$ and $(3k_0, -k_0)$ or $(k_0, -3k_0)$ and $(3k_0, k_0)$ (AR2), $k^2 = 10k_0^2$ (see Fig. 3); and (iii) alternating rolls with basic wave vectors $(-k_0, 2k_0)$ and $(2k_0, k_0)$ or $(k_0, 2k_0)$ and $(-2k_0, k_0)$ (AR3), $k^2 = 5k_0^2$ (see Fig. 4).

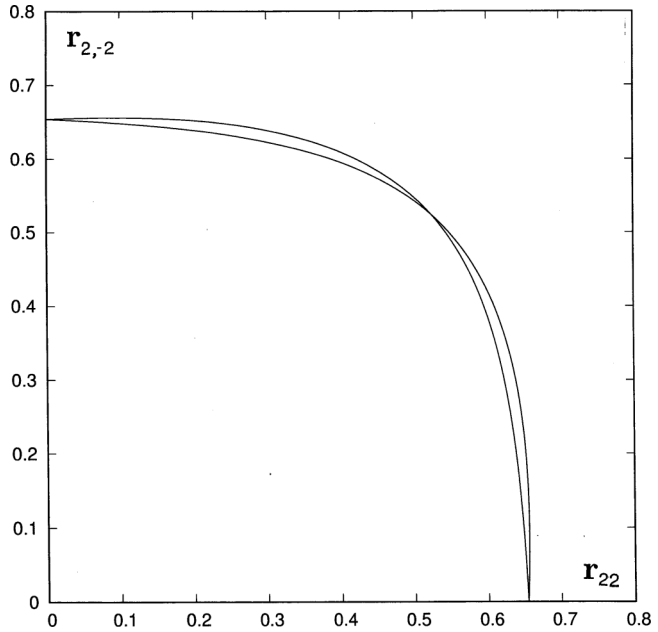

FIG. 6. Phase trajectory in the plane $(r_{22}, r_{2,-2})$ for $M = -2$ and $M_Q = -0.5$ (pattern AR1).

Recall that alternating rolls are a nonlinear superposition of two standing waves oscillating with a certain temporal period T. The amplitudes of these waves oscillate with period $T/2$; the phase shift between oscillations of both standing waves is equal to $T/4$. For the pattern AR1 with basic wave vectors $(2k_0, 2k_0)$ and $(2k_0, -2k_0)$, the temporal evolution of amplitudes $r_{22}(\tau)$ and $r_{2,-2}(\tau)$ is shown in Fig. 5. The phase trajectory in the plane $(r_{22}, r_{2,-2})$ is shown in Fig. 6. Patterns AR2 and AR3 are quite similar to AR1, except for the orientation and lengths of basic vectors.

At a certain time instant $\tau = \tau_0$, $r_{22} = 0$ and pattern AR1 resembles a system of rolls parallel to the diagonal $Y = X$ [see Fig. 2(b)]. At the time instant $\tau = \tau_0 + T/8$, $r_{22} = r_{2,-2}$ and the pattern resembles a system of squares [that time instant is seen especially well for pattern AR3 in Fig. 4(c)]. At the time instant $\tau = \tau_0 + T/4$, $r_{2,-2} = 0$ and pattern AR1 resembles a system of rolls parallel to the diagonal $Y = -X$ [see Fig. 2(d)]. Note that the maxima of amplitudes of both waves are exactly equal:

$$\max_{\tau} r_{2,-2}(\tau) = \max_{\tau} r_{22}(\tau).$$

The quantities $h_{\max,j}$, $j = 1, 2$, oscillate with period $T/4$ (see Fig. 7).

Let us emphasize that the support of the spatial Fourier spectrum of the pattern contains an infinite number of combinations of basic wave vectors with integer coefficients. For instance, pattern AR3 shown in Fig. 4, in addition to basic wave vectors $(2k_0, k_0)$ and $(-k_0, 2k_0)$, includes any wave vectors $\mathbf{k}_{mn} = m(2k_0, k_0) + n(-k_0, 2k_0)$, $m = 0, \pm 1, \ldots$ and $n = 0, \pm 1, \ldots$. The amplitudes of waves corresponding to combinational wave vectors are comparable to the amplitudes of the basic ones; see Fig. 8, where the evolution of amplitudes for waves with wave vectors $(k_0, 3k_0) = (2k_0, k_0) + (-k_0, 2k_0)$ and $(3k_0, -k_0) = (2k_0, k_0) - (-k_0, 2k_0)$ is presented. As shown in [22], the natural evolution of the system from the initial condition corresponding to the mechanical equilibrium state with a small random disturbance leads to pattern AR2 with the squared wave number $k^2 = 10k_0^2$, which corresponds to the disturbance with the maximum growth rate.

Due to the coexistence of three kinds of stable patterns (tristability), the following questions arise: How can one create a definite pattern? Can a weak spatial inhomogeneity of the interfacial

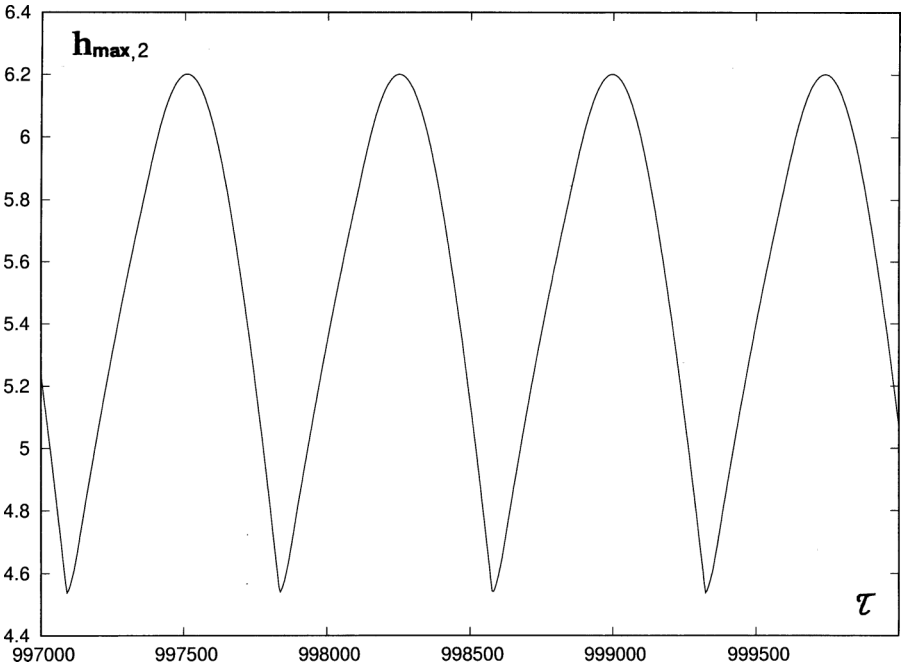

FIG. 7. Temporal evolution of $h_{\max,2}(\tau)$ for $M = -2$ and $M_Q = -0.5$ (pattern AR1).

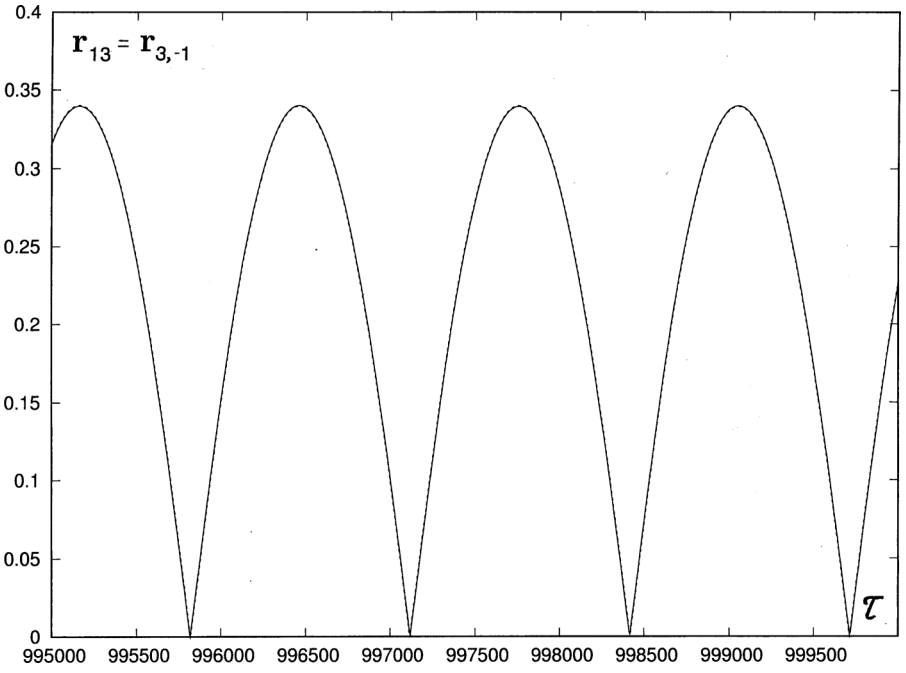

FIG. 8. Temporal evolution of amplitudes $r_{13}(\tau)$ and $r_{3,-1}(\tau)$ for $M = -2$ and $M_Q = -0.5$ (pattern AR3).

heat release or consumption change the evolution of the system significantly and eventually create a pattern of a different kind?

In the case of a monotonic instability, the answer is rather straightforward: In order to create the pattern with the wave vector $\mathbf{k}$, one has to apply the modulation of the parameter of the kind

$$M_Q(\mathbf{X}) = \bar{M}_Q + \Delta M_Q \sin(\mathbf{k}\cdot\mathbf{X} + \phi). \tag{32}$$

The modulation of the parameter creates a disturbance with the wave vector $\mathbf{k}$ which grows due to the instability until the nonlinear stationary pattern with the basic wave vector $\mathbf{k}$ is formed. Then the parameter modulation is eliminated. If the pattern created by modulation is stable, it is retained; otherwise, it evolves towards a pattern with another wave vector. This idea has been successfully applied for stationary roll patterns in the case of Rayleigh-Bénard convection in [5].

Here we are going to create a definite oscillatory pattern by means of a stationary parameter modulation (32). The numerical simulations reveal two different scenarios.

Scenario 1. The oscillatory pattern with the same basic wave vector $\mathbf{k}$ is created.

Specifically, we have performed the simulations with the interfacial heat consumption determined by the formula

$$M_Q(X, Y, \tau) = \begin{cases} \bar{M}_Q + \Delta M_Q \sin[2k_0(X - Y)], & 0 \leqslant \tau \leqslant \tau_m \\ \bar{M}_Q, & \tau > \tau_m, \end{cases} \tag{33}$$

where $\bar{M}_Q = -0.5$ and $\Delta M_Q = 0.05$. For sufficiently large τ_m, a modified AR1 pattern is developed during the time interval $0 \leqslant \tau \leqslant \tau_m$ (see Sec. VI for details). For $\tau > \tau_m$, when ΔM_Q vanishes, the pattern is transformed into AR1 shown in Fig. 2.

Scenario 2. An oscillatory pattern with different basic wave vectors is created.

Specifically, we have applied the parameter modulation

$$M_Q(X, Y, \tau) = \bar{M}_Q + \Delta M_Q \sin[k_0(X + 3Y)], \tag{34}$$

with $\bar{M}_Q = -0.5$ and $\Delta M_Q = 0.012$. One could expect that this kind of modulation will support pattern AR2 with basic wave vectors $\pm(k_0, 3k_0)$ and $\pm(-3k_0, k_0)$. However, after diminishing ΔM_Q in small steps, we have obtained pattern AR3 with basic wave vectors $\pm(k_0, -2k_0)$ and $\pm(2k_0, k_0)$ shown in Fig. 4.

The reason is that the stationary modulation with the wave vector $(k_0, 3k_0)$ forms a bridge between modes with wave numbers $(k_0, -2k_0)$ and $(2k_0, k_0)$. These modes have equal frequencies; therefore a stationary modulation creates a resonant coupling between them. That resonance leads to the formation of pattern AR3.

VI. MODIFICATION OF PATTERNS UNDER THE ACTION OF HEAT CONSUMPTION MODULATION

Let us describe in more detail the modification of patterns caused by the heat consumption modulation.

A. Time-periodic patterns

The inhomogeneity (33) violates the translational invariance of the problem with respect to translations along the direction $(2k_0, -2k_0)$, while the invariance to translations along the direction $(2k_0, 2k_0)$ is retained. Therefore, the Fourier component $c_{2,-2}$ tends to zero (see Fig. 9), while both components s_{22} and c_{22} are generally different from zero (see Fig. 10). Because of the modulation,

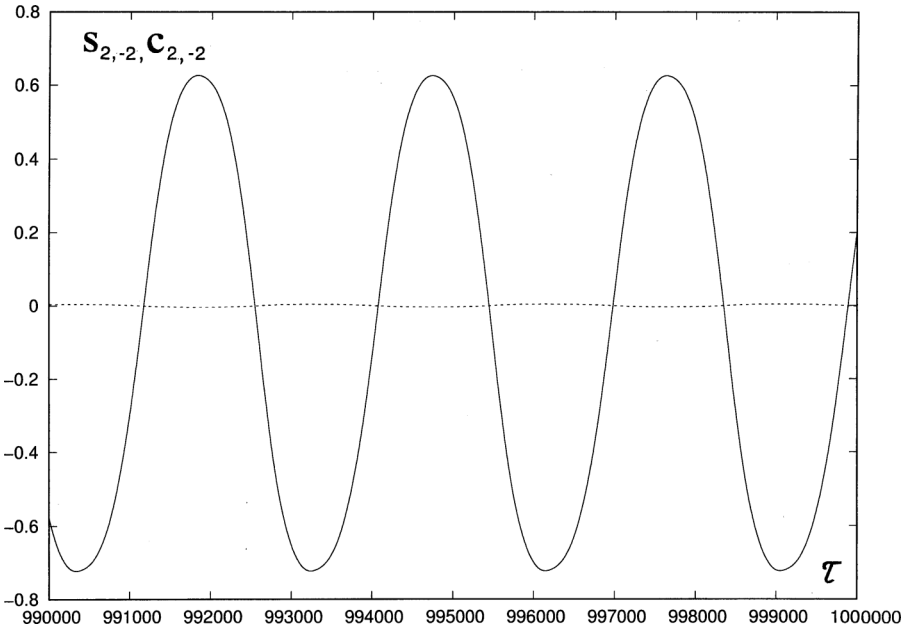

FIG. 9. Temporal evolution of the Fourier component $s_{2,-2}(\tau)$ (solid line) for $M = -2$, $\bar{M}_Q = -0.5$, and $\Delta M_Q = 0.05$ (modified pattern AR1). The component $c_{2,-2}$ (dashed line) tends to 0 at large τ.

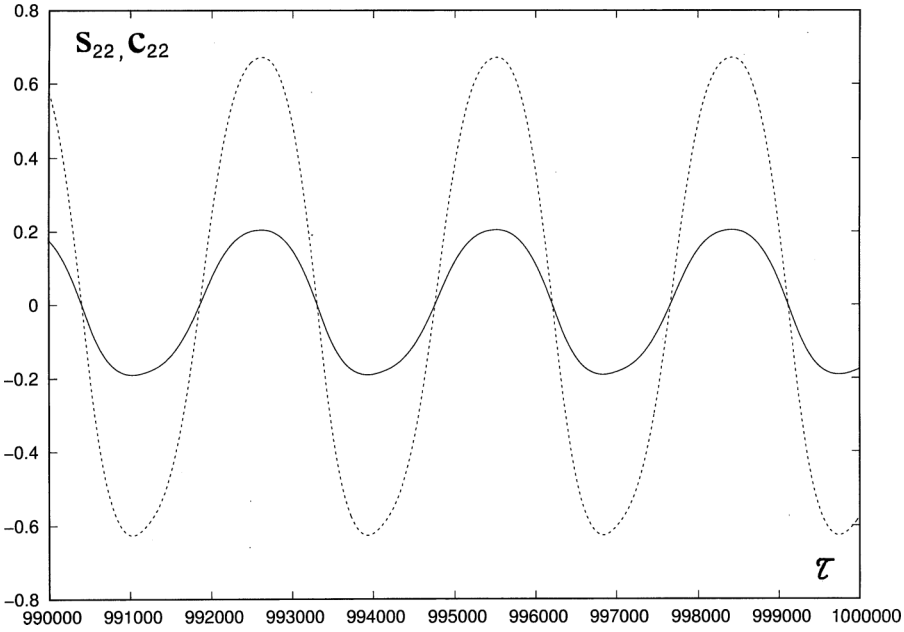

FIG. 10. Temporal evolution of the Fourier components $s_{22}(\tau)$ (solid line) and $c_{22}(\tau)$ (dashed line) for $M = -2$, $\bar{M}_Q = -0.5$, and $\Delta M_Q = 0.05$ (modified pattern AR1).

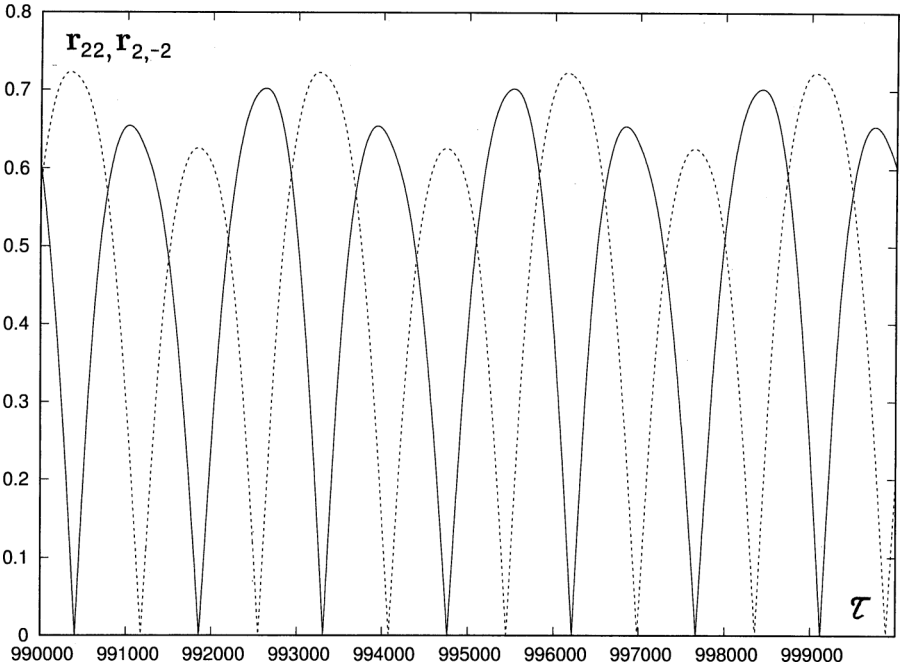

FIG. 11. Temporal evolution of amplitudes $r_{22}(\tau)$ (solid line) and $r_{2,-2}(\tau)$ (dashed line) for $M = -2$, $\bar{M}_Q = -0.5$, and $\Delta M_Q = 0.05$ (modified pattern AR1).

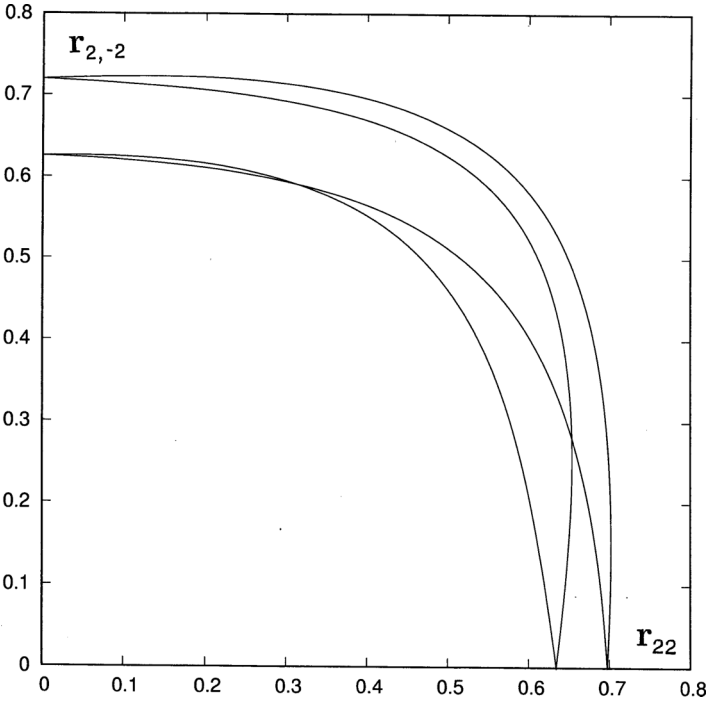

FIG. 12. Phase trajectory in the plane $(r_{22}, r_{2,-2})$ for $M = -2$, $\bar{M}_Q = -0.5$, and $\Delta M_Q = 0.05$ (modified pattern AR1).

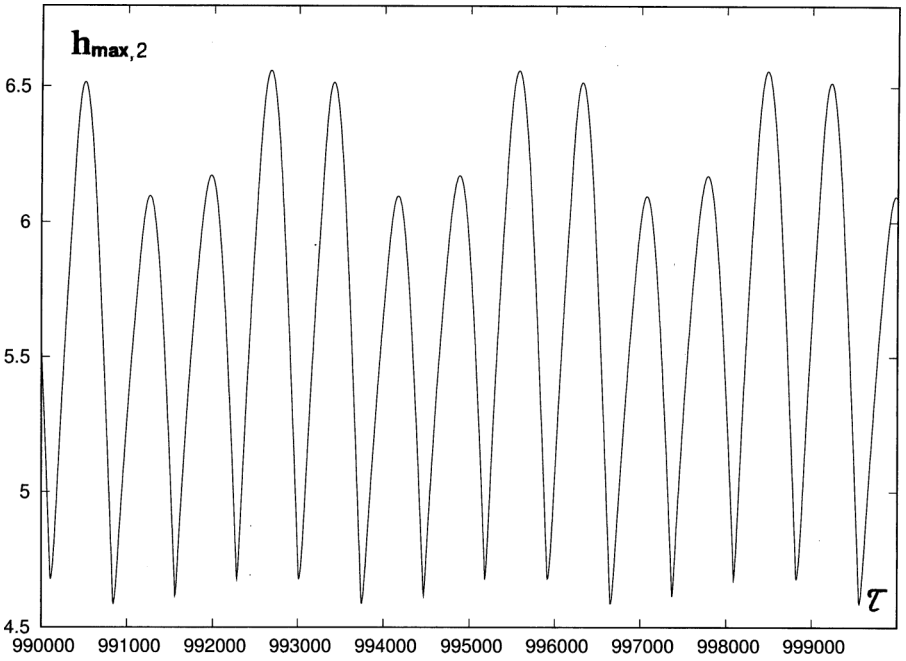

FIG. 13. Temporal evolution of $h_{\max,2}(\tau)$ for $M = -2$, $\bar{M}_Q = -0.5$, and $\Delta M_Q = 0.05$ (modified pattern AR1).

the mean value

$$\bar{s}_{2,-2} = \frac{1}{T}\int_0^T s_{2,-2}(\tau)d\tau \neq 0,$$

while $\bar{s}_{22} = \bar{c}_{22} = 0$. The oscillations of $r_{22}(\tau)$ and $r_{2,-2}(\tau)$ are shown in Figs. 11 and 12. Their period coincides with the oscillation period of Fourier components s_{22}, c_{22}, and $s_{2,-2}$. The quantities $h_{\max,j}(\tau)$, $j = 1, 2$, oscillate with the same period T (see Fig. 13).

Snapshots of contour lines are shown in Fig. 14. In addition, we considered the influence of the perturbation (34) on the pattern AR3 with the basic wave vectors $(-k_0, 2k_0)$ and $(2k_0, k_0)$. The components $(k_0, 3k_0)$ and $(3k_0, -k_0)$ are generated by both the nonlinear interaction of basic Fourier components (see Fig. 8) and the external perturbation.

As explained above, because of the modulation, $c_{13} = 0$ and $\bar{s}_{13} \neq 0$ (see Fig. 15). The evolution of amplitudes r_{13} and $r_{3,-1}$ is shown in Figs. 16 and 17. The oscillation period of $h_{\max,j}$, $j = 1, 2$, coincides with that of Fourier components s_{13}, $s_{3,-1}$, and $c_{3,-1}$ (see Fig. 18).

B. Quasiperiodic oscillations

The oscillatory patterns described in Sec. VI A keep their symmetry with respect to two orthogonal symmetry axes in the course of oscillations (see Fig. 14). Let us discuss now the action of modulation (27) incompatible with the reflection symmetry of the pattern. For instance, let us consider the action of the modulation

$$M(X, Y, \tau) = \bar{M}_Q + \Delta M_Q \sin k_0 X \tag{35}$$

on pattern AR1. Let us introduce new variables $\bar{X} = (X + Y)/\sqrt{2}$ and $\bar{Y} = (Y - X)/\sqrt{2}$. In the absence of modulation, with an appropriate shift of the origin, pattern AR1 is symmetric with respect

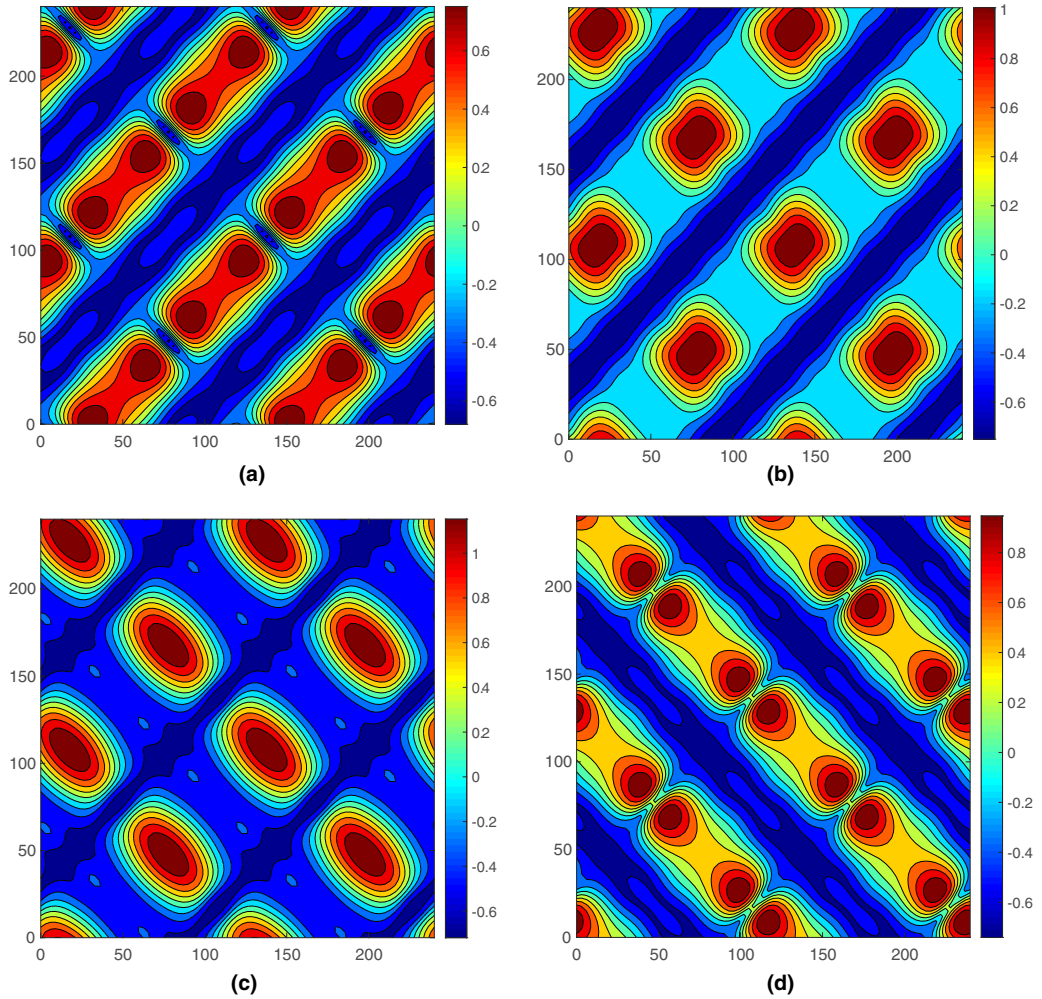

FIG. 14. Snapshots of contour lines of $h_1(X, Y, \tau) - 1$ for modified alternating rolls with basic wave vectors $(2k_0, 2k_0)$ and $(2k_0, -2k_0)$ (modified pattern AR1) for $M = -2$, $\bar{M}_Q = -0.5$, $\Delta M_Q = 0.05$, and (a) $\tau = 1\,500\,250$, (b) $\tau = 1\,500\,500$, (c) $\tau = 1\,500\,750$, and (d) $\tau = 1\,501\,000$.

to each of the transformations

$$\bar{X} \to -\bar{X}, \quad \bar{Y} \to -\bar{Y}. \tag{36}$$

Within that pattern, waves moving in positive and negative directions of axes $\tilde{X}$ and $\tilde{Y}$ have equal amplitudes and frequencies, and thus the pattern is time periodic. The disturbance

$$\Delta M_Q \sin k_0 X = \Delta M_Q \sin[k_0(\bar{X} - \bar{Y})/\sqrt{2}]$$

violates symmetry (36). Therefore, waves moving in the positive and negative directions of axes $\bar{X}$ and $\bar{Y}$ have different amplitudes and frequencies. The superposition of those waves leads to the amplitude pulsation on the background of a pattern moving as a whole. Generally, the pulsation period and the time needed for passing the distance L by the moving pattern are incommensurate; therefore the flow is quasiperiodic in time. An example of quasiperiodic oscillations of Fourier components $s_{22}(\tau)$ and $c_{22}(\tau)$ and the corresponding phase trajectory in the plane (s_{22}, c_{22}) are

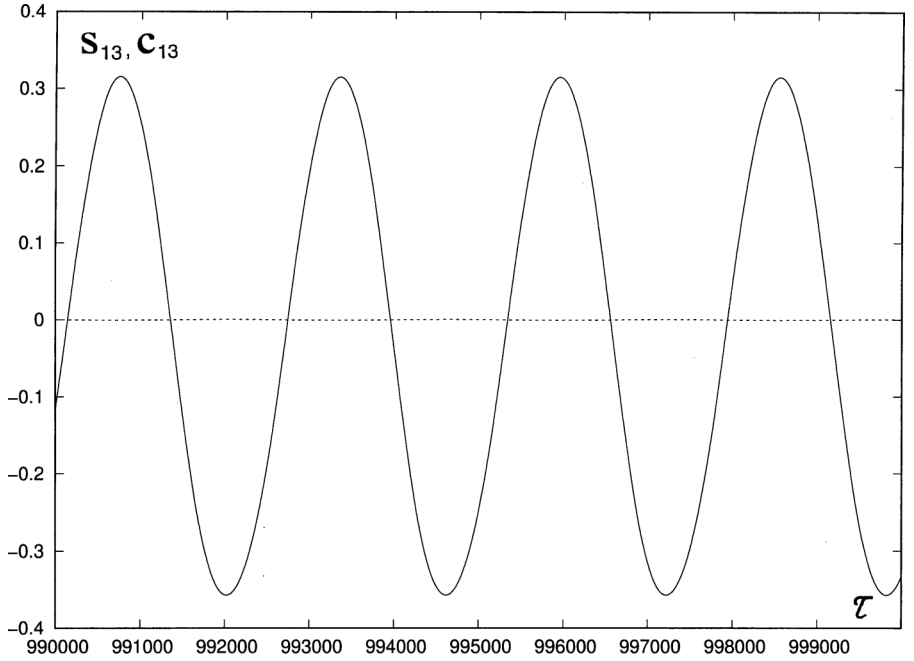

FIG. 15. Temporal evolution of Fourier component $s_{13}(\tau)$ (solid line) and plot of $c_{13}(\tau) = 0$ (dashed line) for $M = -2$, $\bar{M}_Q = -0.5$, and $\Delta M_Q = 0.012$ (modified pattern AR3).

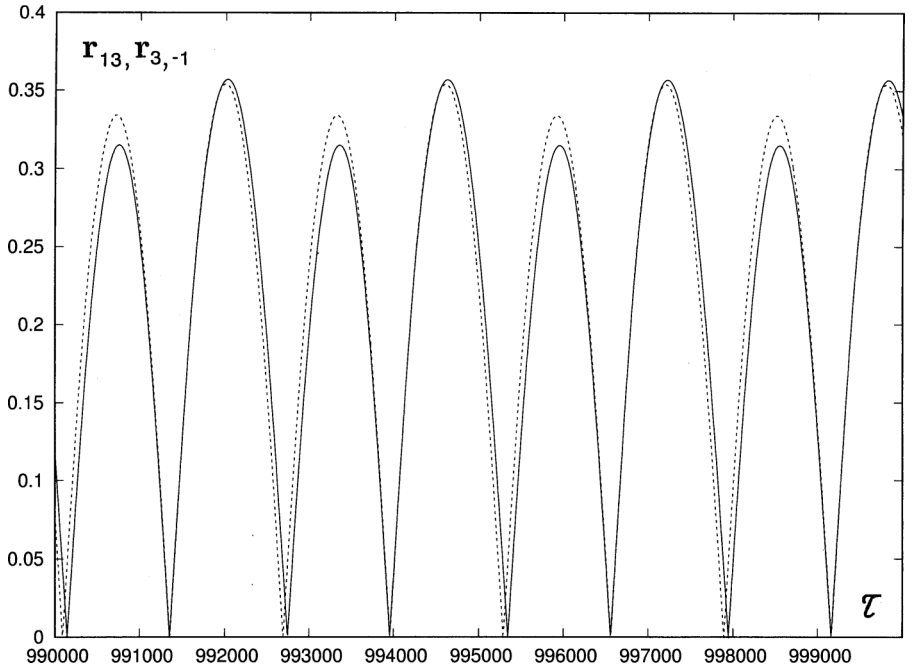

FIG. 16. Temporal evolution of amplitudes $r_{13}(\tau)$ (solid line) and $r_{3,-1}(\tau) = 0$ (dashed line) for $M = -2$, $\bar{M}_Q = -0.5$, and $\Delta M_Q = 0.012$ (modified pattern AR3).

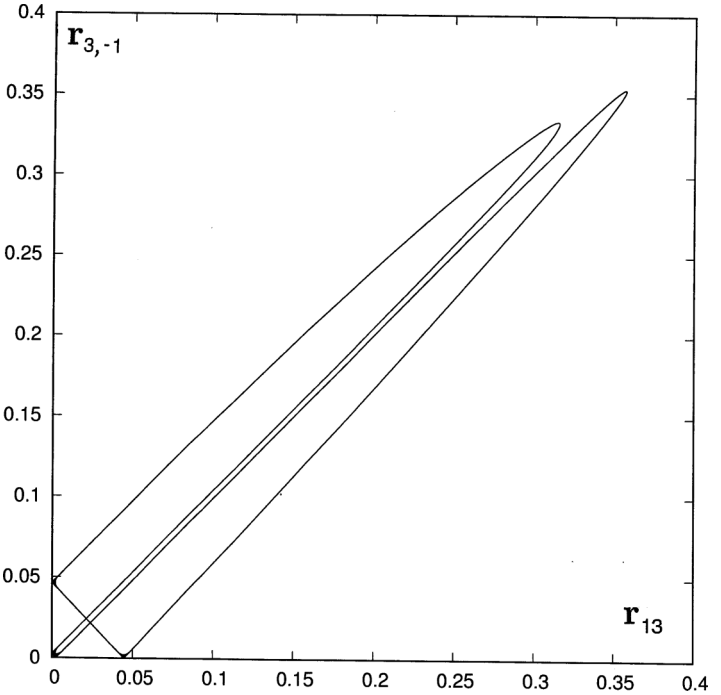

FIG. 17. Phase trajectory in the plane $(r_{13}, r_{3,-1})$ for $M = -2$, $\bar{M}_Q = -0.5$, and $\Delta M_Q = 0.012$ (modified pattern AR3).

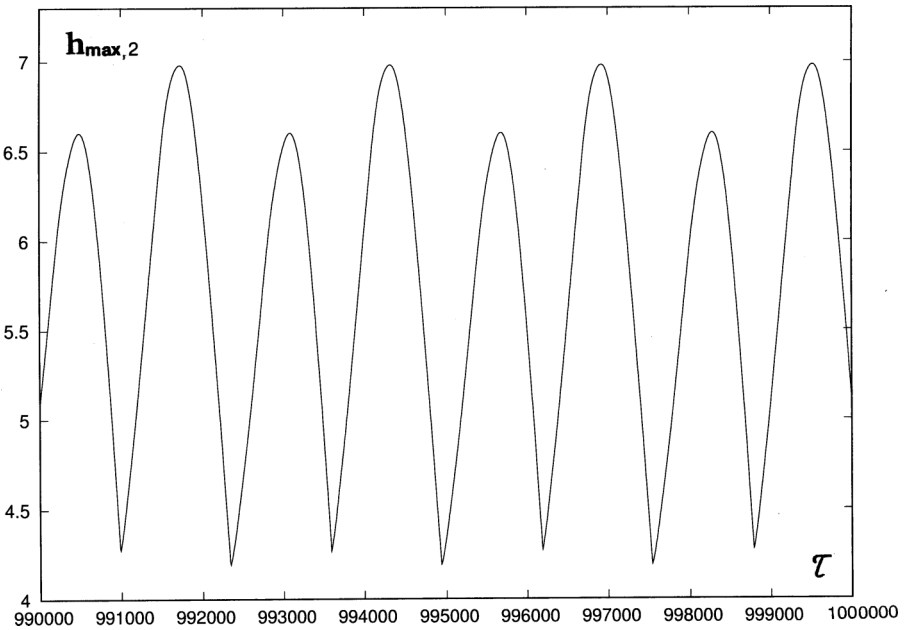

FIG. 18. Temporal evolution of $h_{\max,2}(\tau)$ for $M = -2$, $\bar{M}_Q = -0.5$, and $\Delta M_Q = 0.012$ (modified pattern AR3).

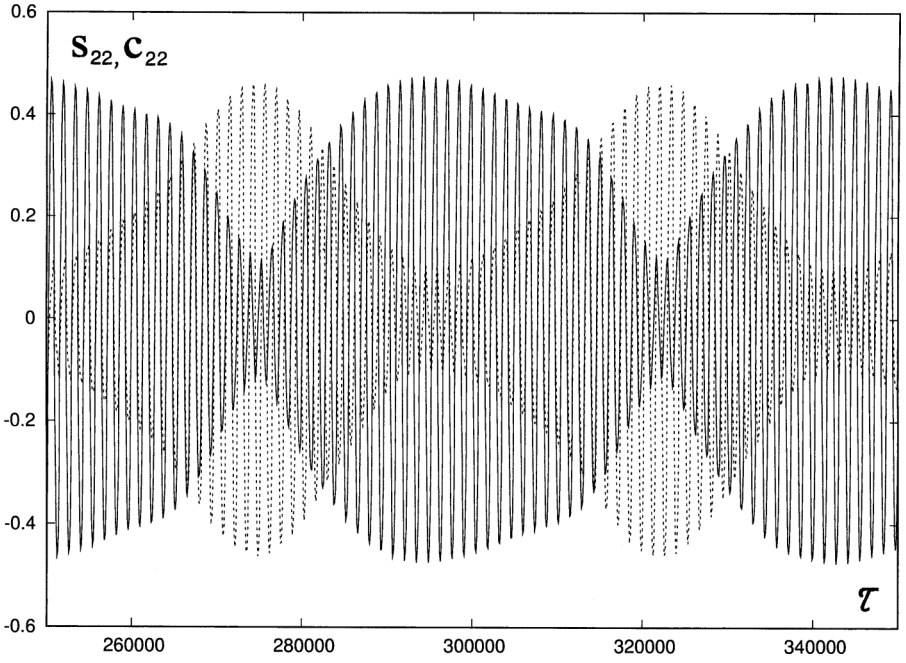

FIG. 19. Temporal evolution of Fourier components $s_{22}(\tau)$ (solid line) and $c_{22}(\tau)$ (dashed line) for $M = -5$, $M_Q = -0.75$, and $\Delta M_Q = 0.25$ (quasiperiodic oscillations).

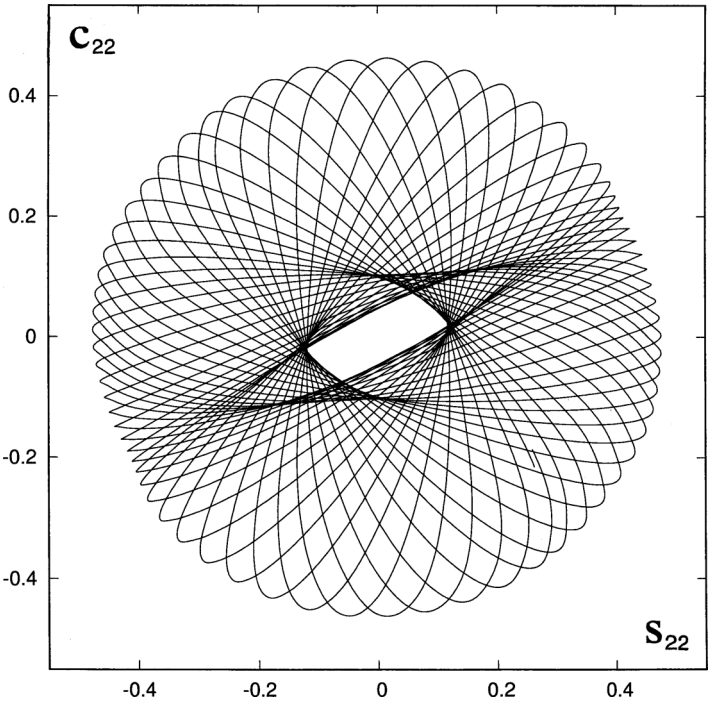

FIG. 20. Phase trajectory in the plane (s_{22}, c_{22}) for $M = -5$, $M_Q = -0.75$, and $\Delta M_Q = 0.25$ (quasiperiodic oscillations).

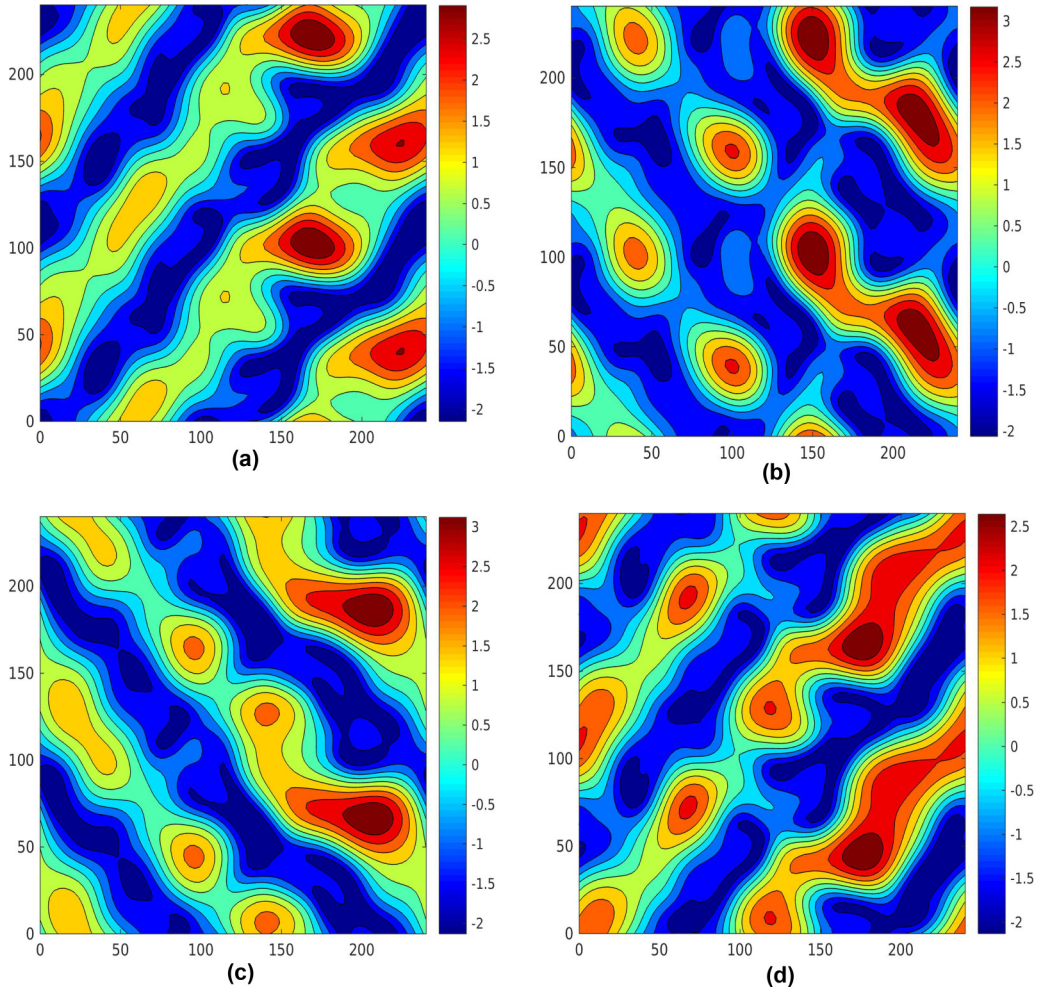

FIG. 21. Snapshots of contour lines of $h_2(X, Y, \tau) - h$ for quasiperiodic oscillations for $M = -5$, $\bar{M}_Q = -0.75$, $\Delta M_Q = 0.25$, and (a) $\tau = 2\,100\,140$, (b) $\tau = 2\,100\,200$, (c) $\tau = 2\,100\,220$, and (d) $\tau = 2\,100\,300$.

shown in Figs. 19 and 20. The oscillations of components $s_{2,-2}(\tau)$ and $c_{2,-2}(\tau)$ are similar. Snapshots of contour lines are shown in Fig. 21.

VII. CONCLUSION

We have considered Marangoni waves in two-layer films under the action of spatial modulation of the Marangoni number M_Q corresponding to the heat source or sink at the interface. In the case of multistability, the spatial modulation can be used for the creation of a pattern with a definite spatial structure. The response of the oscillatory system to a stationary spatially periodic inhomogeneity turned out to be nontrivial. The periodic stationary modulation of parameter M_Q with wave vector $\mathbf{k}$ does not always create an oscillatory pattern with $\mathbf{k}$ as one of the basic wave vectors. That modulation can create a pattern with some different basic wave vectors $\mathbf{k}_1$ and $\mathbf{k}_2$ such that $\mathbf{k} = \mathbf{k}_2 - \mathbf{k}_1$ serves as a bridge for a resonance between the oscillations with basic wave vectors.

Modification of alternating roll patterns of different scales due to the Marangoni number modulation has been investigated. It has been shown that the violation of the reflection symmetry of the pattern by its spatial heat release modulation can lead to a quasiperiodic temporal evolution.

ACKNOWLEDGMENT

This research was supported by the Israel Science Foundation (Grant No. 843/18).

[1] M. C. Cross and P. C. Hohenberg, Pattern formation outside of equilibrium, Rev. Mod. Phys. **65**, 851 (1993).
[2] I. S. Aranson and L. Kramer, The world of the complex Ginzburg-Landau equation, Rev. Mod. Phys. **74**, 99 (2002).
[3] A. S. Mikhailov and K. Showalter, Control of waves, patterns and turbulence in chemical systems, Phys. Rep. **425**, 79 (2006).
[4] *Handbook of Chaos Control*, 2nd ed., edited by E. Schöll and H. G. Schuster (Wiley-VCH, Weinheim, 2008).
[5] M. M. Chen and J. A. Whitehead, Evolution of two-dimensional periodic Rayleigh convection cells of arbitrary wave-numbers, J. Fluid Mech. **31**, 1 (1968).
[6] L. P. Vozovoi and A. A. Nepomnyashchy, in *Hydrodynamics*, edited by E. M. Zhukhovitskii (Perm State Pedagogical Institute, Perm, 1974), Pt. 7, p. 107.
[7] L. P. Vozovoi and A. A. Nepomnyashchy, On the stability of spatially periodic convective flows in the vertical layer with curved boundaries, J. Appl. Math. Mech. **43**, 1080 (1979).
[8] P. Coullet, C. Elphick, and D. Repaux, Nature of Spatial Chaos, Phys. Rev. Lett. **58**, 431 (1987).
[9] L. M. Pismen, Bifurcation of Quasiperiodic and Nonstationary Patterns under External Forcing, Phys. Rev. Lett. **59**, 2740 (1987).
[10] R. Manor, A. Hagberg, and E. Meron, Wave-number locking in spatially force pattern-forming systems, Europhys. Lett. **83**, 10005 (2008).
[11] G. Freund, W. Pesch, and W. Zimmermann, Rayleigh-Bénard convection in the presence of spatial temperature modulations, J. Fluid Mech. **673**, 318 (2011).
[12] Y. Mau, L. Haim, A. Hagberg, and E. Meron, Competing resonances in spatial forced pattern-forming systems, Phys. Rev. E **88**, 032917 (2013).
[13] L. Haim, Y. Mau, and E. Meron, Spatial forcing of pattern-forming systems that lack inversion symmetry, Phys. Rev. E **90**, 022904 (2014).
[14] S. Weiss, G. Seiden, and E. Bodenschatz, Resonance patterns in spatially forced Rayleigh-Bénard convection, J. Fluid Mech. **756**, 293 (2014).
[15] A. A. Nepomnyashchy, Spatially modulated convective motions in a vertical layer with curved boundaries, J. Appl. Math. Mech. **52**, 677 (1988).
[16] B. A. Malomed, Ramp-induced wave-number selection for traveling waves, Phys. Rev. E **47**, R2257 (1993).
[17] C. Utzny, W. Zimmermann, and M. Bär, Resonant spatio-temporal forcing of oscillatory media, Europhys. Lett. **57**, 113 (2002).
[18] M. Hammele and W. Zimmermann, Harmonic versus subharmonic patterns in a spatially forced oscillating chemical reaction, Phys. Rev. E **73**, 066211 (2006).
[19] S. I. Abarzhi, O. Desjardins, A. Nepomnyashchy, and H. Pitsch, Influence of parametric forcing on the nonequilibrium dynamics of wave patterns, Phys. Rev. E **75**, 046208 (2007).
[20] A. A. Nepomnyashchy and S. I. Abarzhi, Monochromatic waves induced by large-scale parametric forcing, Phys. Rev. E **81**, 037202 (2010).
[21] A. A. Nepomnyashchy and I. B. Simanovskii, Marangoni waves in two-layer films under the action of spatial temperature modulation, J. Fluid Mech. **805**, 322 (2016).

[22] A. A. Nepomnyashchy and I. B. Simanovskii, Novel criteria for the development of monotonic and oscillatory instabilities in a two-layer film, Phys. Fluids **29**, 092104 (2017).
[23] C. N. R. Rao, *Chemical Applications of Infrared Spectroscopy* (Academic, New York, 1963).
[24] A. K. Thokchom, A. Gupts, P. J. Jaijus, and A. Singh, Analysis of fluid flow and particle transport in evaporating droplets exposed to infrared heating, Int. J. Heat Mass Transfer **68**, 67 (2014).
[25] I. B. Simanovskii and A. A. Nepomnyashchy, *Convective Instabilities in Systems with Interface* (Gordon and Breach, London, 1993).
[26] S. H. Davis, Thermocapillary instabilities, Annu. Rev. Fluid Mech. **19**, 403 (1987).
[27] A. Oron, S. H. Davis, and S. G. Bankoff, Long-scale evolution of thin liquid films, Rev. Mod. Phys. **69**, 931 (1997).
[28] A. A. Nepomnyashchy and I. B. Simanovskii, Nonlinear Marangoni waves in a two-layer film in the presence of gravity, Phys. Fluids **24**, 032101 (2012).
[29] C. Burkersroda, A. Prakash, and J. Koster, Interfacial tension between fluorinert and silicone oil, Microgravity Q. **4**, 93 (1994).
[30] M. M. Degen, P. W. Colovas, and C. D. Andereck, Time-dependent patterns in the two-layer Rayleigh-Bénard system, Phys. Rev. E **57**, 6647 (1998).
[31] P. Géoris, M. Hennenberg, G. Lebon, and J. C. Legros, Investigation of thermocapillary convection in a three-liquid-layer systems, J. Fluid Mech. **389**, 209 (1999).
[32] I. Nejati, M. Dietzel, and S. Hardt, Conjugated liquid layers driven by the short-wavelength Bénard-Marangoni instability: Experiment and numerical simulation, J. Fluid Mech. **783**, 46 (2015).